Numerical investigation of evaporation of a single ethanol/iso-octane droplet

ARTICLE *in* FUEL · MAY 2013

Impact Factor: 3.41 · DOI: 10.1016/j.fuel.2013.01.003

1 AUTHOR:

R. Banerjee
Indian Institute of Technology Hyderabad
25 PUBLICATIONS **67** CITATIONS

Fuel 107 (2013) 724–739

Contents lists available at SciVerse ScienceDirect

Fuel

journal homepage: www.elsevier.com/locate/fuel

Numerical investigation of evaporation of a single ethanol/iso-octane droplet

R. Banerjee *

Department of Mechanical Engineering, Indian Institute of Technology Hyderabad, Yeddumailaram, AP 502 205, India

HIGHLIGHTS

- Non-uniform vortices inside liquid droplet due to shearing interaction with the gas phase.
- Droplet temperature has the most significant effect on evaporation rate.
- Droplet composition and predominant evaporating species affects overall droplet temperature.
- Droplet composition affects rate of change in droplet diameter.

ARTICLE INFO

Article history:
Received 17 September 2012
Received in revised form 15 December 2012
Accepted 2 January 2013
Available online 25 January 2013

Keywords:
Droplet evaporation
Two-phase flow
VOF
Multicomponent fluid

ABSTRACT

Numerical study has been performed to analyse evaporation of a single droplet composed of a binary mixture of ethanol and iso-octane. The Navier–Stokes equations are solved in conjunction with VOF multiphase model to track the liquid/gas interface over time. Ethanol and iso-octane form a highly non-ideal mixture and therefore the UNIFAC group contribution method was used to determine the vapour–liquid equilibrium (VLE). Source terms due to interfacial mass transfer were implemented in the continuity, momentum, energy and species equations. Commercial computational fluid dynamics solver, Ansys Fluent 13.0 was used in this study. VLE, mixture transport properties and source terms due to interfacial mass transfer were implemented using user defined functions. Parametric study to analyse the effect of free stream temperature and composition, droplet temperature and composition was performed.

1. Introduction

Multicomponent droplet evaporation is important in many industrial and engineering applications and once such application is evaporation of fuel droplets during fuel injection and atomization [1]. Due to environmental concerns, alcohol blended gasoline is being increasingly considered as an alternative fuel for SI engines [2]. Several experimental and numerical studies have been performed to understand the fuel injection process and has been previously reviewed by Drake and Haworth [3] and Jiang et al. [4]. Godsave [5] and Spalding [6] were the first to propose an evaporation model based on the d^2-law for a single fuel droplet, where the droplet temperature remained constant at the wet bulb temperature. Law [7] proposed an evaporation model based on the Infinite Conduction Model, where the temperature changed with time but was spatially constant inside the droplet. Later this restriction on constant spatial temperature distribution inside the droplet was relaxed using the Finite Conduction Model [8]. Sirignano and Law [9] included effect of internal circulation on droplet evaporation. Haywood et al. [10,11] have performed detailed flow field analysis for axisymmetric flow by solving the Navier–Stokes equation for stationary and deforming droplets. Miller et al. [12] compared equilibrium and non-equilibrium evaporation models for many-droplet gas–liquid flow. More recently, Abarham and Wichman [13] studied evaporation/condensation of a single droplet in presence of background fuel vapour.

The above studies were performed for single component droplets. However, fuels used in many engineering applications are complex multicomponent fluids. Researchers have used various models to represent heat and mass transfer for multicomponent fluids. Bhattacharya et al. [14] have performed a theoretical investigation on a bi-component hydrocarbon droplet composed of n-hexane and n-hexadecane. Their study included the effect of finite diffusion and rapid mixing on droplet evaporation. Sezen [15] derived analytical expression for a single multicomponent droplet based on Infinite Conduction Model. Nadykto et al. [16] derived expressions for mass flux from multicomponent droplet evaporation and condensation under non-isothermal condition. Zeng and Lee [17] used a third order polynomial to model temperature and concentration profiles for multicomponent fuel film vaporization. Yao [18] used film theory to model multicomponent droplet evaporation for high and low pressure environments. Sazhin and his group have reported a number of studies on multi-component

* Tel.: +91 40 2301 6015.
E-mail address: rajabanerjee@iith.ac.in

0016-2361/$ - see front matter © 2013 Elsevier Ltd. All rights reserved.
http://dx.doi.org/10.1016/j.fuel.2013.01.003

Nomenclature

C_p	specific heat (J/kg-K)
D, D_{ij}	binary diffusivity (m/s^2)
E	specific energy (J/kg)
$\boldsymbol{F}$	body force (N/m^3)
$\mathbf{g}$	acceleration due to gravity (m/s^2)
h	enthalpy (J/kg)
$\boldsymbol{J}$	species flux (kg/m^2-s)
k	thermal conductivity (W/m-k)
m_i'''	mass transfer/volume (kg/m^3)
p	pressure (Pa)
S_e	energy source term (W/m^3)
S_m	momentum source term (N/m^3)
$S_{\alpha q}$	source term VOF eq. (kg/m^3)
T	temperature (K)
t	time (s)
u, $\mathbf{u}$	velocity (m/s)
U_∞	free stream velocity (m/s)
V	volume (m^3)
X	liquid mole fraction
x	gas phase mole fraction
Y	liquid phase mass fraction
y	gas phase mass fraction

Greek symbols

α	volume fraction
γ	activity coefficient
μ	viscosity (Pa s)
ρ	density (kg/m^3)
σ	surface tension (N-m)

Subscripts

b	bulk
d	droplet
dp	dew point
g	gas phase
i	initial value
l	liquid phase
q	qth phase
s	saturated value
vap	vapour
∞	free stream

Superscript

i,j	i or jth species

Abbreviations

VOF	Volume of Fluid
UNIFAC	Universal Functional Activity Coefficient
SIMPLEC	Semi-Implicit Method for Pressure Linked Equations-Consistent

droplet evaporation. They have reported evaporation models based on analytical solutions of heat conduction and species diffusion for two-component droplet [19] and arbitrary number of species [20]. They have also reported the effect of replacing complex multicomponent fuel with relatively few quasi-components having average properties similar to the representative group of actual components [21].They included effects of temperature gradient and quasi-component diffusion inside the droplet. However, according to Aggarwal and Mongia [22], evaporation characteristics of a bi-component fuel can be effectively represented by a single surrogate component fuel (50% boiling point) at high pressures because evaporation is more sensitive to droplet heating models than to droplet composition.

In all the above mentioned multicomponent evaporation models, the number of components that have been used is relative few in number. However, petroleum fuels are complex multicomponent fluids which are composed of several hundred different components and therefore tracking all the components becomes computationally very expensive. Researchers have used alternative methods to represent such complex multicomponent fluids. Burger et al. [23] have used Distillation Curve Model (DC model) to represent aviation fuels like JP-4, Jet-A1, etc. The DC model describes fractional boiling during droplet evaporation process as a function of the mean molar molecular weight of the fuel. As the model is based on algebraic equations, it is computationally less expensive. In a similar approach, multicomponent fuel composition can be represented using Continuous Thermodynamics [24,25]. Here the fuel composition is represented using a probability distribution function based on one or more macro-properties. Researchers [26–28] have used this approach to solve transport equations to determine evaporation rate and composition time history of multicomponent droplets. In all the above mentioned studies, the effect of droplet deformation was not taken into account.

Alcohols like ethanol have a relatively high polarity compared to hydrocarbons. Therefore, a mixture of alcohol and hydrocarbons is highly non-ideal. It has been shown previously [29] that a binary mixture of ethanol and iso-octane has a higher vapour pressure compared to its individual components. Therefore, interfacial mass flux of such mixtures is also correspondingly higher. Droplet shape, thermal and mass diffusion is expected to have a strong bearing on the evaporation rate of alcohol and hydrocarbon mixtures. Interface of two immiscible fluids has been tracked using different interface tracking methods like VOF [30], Level-Set [31], Front-tracking or immersed boundary method [32] and their variants [33]. The VOF method has been previously used to simulate heat and mass transfer in droplets [34,35], bubbles [36] and film boiling [37,38]. More recently, Tanguy et al. [39] reported evaporation of a 2D moving droplet using Level-Set/Ghost Fluid Method; Schlottke and Weigand [40] used VOF method to perform DNS studies on evaporating 3D droplet with high density ratio; and Strotos et al. [41] again used VOF method to study evaporation of a bi-component 3D droplet suspended from a spherical suspender. In their analysis they used a binary mixture of n-heptane and n-decane in various proportions. As various aspects of droplet evaporation have been studied for several decades, the literature review presented above can no way be considered exhaustive and therefore has been restricted to the context to the study reported here. The author would suggest excellent review articles reported elsewhere [42–44] for more detailed discussion on various droplet evaporation models.

The present study is aimed at understanding the effects of droplet internal and near vicinity flow physics for non-ideal multicomponent droplet evaporation time history. In keeping with the aforementioned objective, a 2D droplet composed of a binary mixture of ethanol and iso-octane has been investigated in this paper. This work is an extension of a previous study reported elsewhere [45]. An evaporation model suitable for such mixtures has been

implemented. The moving liquid/gas interface was tracked using VOF multiphase model. The evaporation model was validated against experimental data for a single component droplet from open literature. Due to the non-ideal nature of the mixture, UNIFAC group contribution method was used to determine the activity coefficient for vapour–liquid equilibrium calculations. A parametric study was performed to record the effect of gas phase temperature and composition; droplet temperature and composition on evaporation rate time-history.

2. Mathematical formulation

2.1. Conservation equations

Liquid gas interface was tracked using VOF multiphase model which is expressed as,

$$\frac{1}{\rho_q}\left[\frac{\partial}{\partial t}(\alpha_q\rho_q)+\nabla\cdot(\alpha_q\rho_q u_q)=S_{\alpha q}\right] \tag{1}$$

where volume fraction of all the phases is constrained as,

$$\sum_{q=1}^{n}\alpha_q=1$$

VOF is a fixed grid technique and while using this model, a single set of momentum equation is shared among all the phases. As there are only two phases in this study, $n = 2$. Transport properties appearing in the various conservation equations are determined based on the volume fraction of all the phases present in a given computation cell as illustrated below:

$$\rho=\sum_{q=1}^{n}\alpha_q\rho_q \tag{2}$$

The geometric reconstruction algorithm, which represents the interface between the two phases using a piecewise-linear profile, was used to determine the face fluxes for the VOF model. It assumes that the interface between the two-fluids has a linear slope within each cell and uses this property to calculate the advection of fluid through the cell faces using a geometric reconstruction scheme.

A single momentum equation is solved in the whole flow domain while using VOF model and is expressed as,

$$\frac{\partial(\rho\boldsymbol{u})}{\partial t}+\nabla\cdot(\rho\boldsymbol{u}\boldsymbol{u})=-\nabla\rho+\nabla\cdot[\mu(\nabla\boldsymbol{u}+\nabla\boldsymbol{u}^T)]+\boldsymbol{F}+S_m \tag{3}$$

The body force term, $\boldsymbol{F}$, is due to pressure jump condition appearing at the liquid/gas interface due to surface tension. This pressure jump term is determined using Continuous Surface Force (CSF) model [46]. It is expressed as,

$$p_\alpha=\sigma\nabla\cdot\left(\frac{\nabla\alpha_q}{|\nabla\alpha_q|}\right) \tag{4}$$

A single energy equation is solved in the whole flow domain,

$$\frac{\partial(\rho E)}{\partial t}+\nabla\cdot[\boldsymbol{u}(\rho E+p)]=\nabla\cdot\left(k\nabla T-\sum_j h^j\boldsymbol{J}^j\right)+S_e \tag{5}$$

where energy, E, is mass-averaged as shown below,

$$E=\frac{\sum_{q=1}^{n}\alpha_q\rho_q E_q}{\sum_{q=1}^{n}\alpha_q\rho_q}$$

Phase specific species equation is solved with VOF model and is expressed as,

$$\frac{\partial(\rho_q\alpha_q y_q^i)}{\partial t}+\nabla\cdot(\rho_q\alpha_q\boldsymbol{u}y_q^i)=\nabla\cdot(\rho_q\alpha_q D^i\nabla y_q^i)+S^i \tag{6}$$

and binary diffusion is given as,

$$D^i=\frac{1-x^i}{\sum_{i,j=i}x^j/D_{ij}}$$

As the gas phase is a tertiary mixture of ethanol vapour, iso-octane vapour and air, two species equations are solved in the gas phase. One species equation is solved to track the change in the liquid phase composition.

2.2. Interface conditions

Due to the volatile nature of the fluid, the droplet will evaporate when exposed to a hot stream of air. Interfacial mass transfer is determined from the ith species mass fraction gradient at the liquid/gas interface as shown below,

$$m_i'''=-\rho_g D^i\nabla y^i\cdot\nabla\alpha_g \tag{7}$$

The interfacial mass transfer term is zero in the whole domain, except at the liquid/gas interface. Due to droplet evaporation, there will be jump terms in the liquid/gas interface and these are implemented as source terms in the conservation equations. The source terms are listed in Table 1. A detailed explanation of the source terms is given in the author's earlier works [47] and [29].

2.3. Vapour/liquid equilibrium calculations

Due the relatively high polarity of the ethanol molecule, a binary mixture of ethanol and iso-octane form a non-deal mixture. Therefore, the partial pressure of the mixture at the liquid/gas interface strongly depends on droplet composition. Unlike in [29], the liquid/gas interface is assumed to be at thermodynamic equilibrium in the present study. Hence the evaporation efficiency term used in [29] was taken to be unity. The liquid/gas interface vapour mole fraction of the ith species is therefore determined using the following expression,

$$x^i=\frac{\gamma^i X^i P^i_{vap}}{P} \tag{8}$$

where γ^i is the activation coefficient and is determined using UNIFAC method as given in [48]. During evaporation, the maximum temperature that a droplet can attain under thermodynamic equilibrium is the dew point temperature. The dew point temperature for ethanol/iso-octane mixture at 1 bar pressure can be expressed using the polynomial,

$$T_{dp}=371.97-22.348X-202.99X^2+372.28X^3-167.54X^4 \tag{9}$$

where X is the mole fraction of ethanol in the droplet. The R^2 value of this polynomial is 0.99.

Table 1
Source terms appearing in conservation equations.

Equations	Source terms
VOF (liquid phase)	$S_{\alpha l}=-\sum_i^n m_i'''$
VOF (gas phase)	$S_{\alpha g}=\sum_i^n m_i'''$
Momentum	$S_m=(1-2\alpha_l)\sum_i^n m_i'''\boldsymbol{u}$
Energy	$S_e=-\rho\sum_i^n\frac{m_l'''}{\rho_l}h_{fg}^i$
Species (gas phase)	$S^i=m_i'''$
Species (liquid phase)	$S^i=MW_{avg}\left[\frac{m_{C_2H_5OH}'''}{MW_{C_2H_5OH}}-\frac{m_{C_8H_{18}}'''}{MW_{C_8H_{18}}}\right]$
	$MW_{avg}=\sum_{i=1}^{2}X_iMW_i$

3. Solution method

Commercial CFD software Ansys Fluent 13 was used to perform the numerical simulations in this study. Ansys Fluent uses control volume method to discretize the governing equations on an unstructured grid. Second order upwind scheme was used to discretize the transport equations. Body force weighted pressure discretization scheme was used to take into account body force due to gravity. SIMPLEC algorithm was used for pressure–velocity coupling. To take into account the non-physical values of vapour mass fraction gradient at the liquid/gas interface due to discontinuity in the species equation, dummy variables were used to determine the gradient at the liquid/gas interface, which in turn were used to determine the evaporation rate. A detailed description on the implementation of the dummy variables is given in [29]. Mixture models described previously [29], were used to determine the transport properties in the liquid and gas phases. The thermo-physical properties of the individual working fluids are given in Table 2.

3.1. Validation

The evaporation model was validated against experimental data reported in open literature. Evaporation data of a single heptane droplet suspended from the surface of a sphere of diameter 400 μm, as reported by Daïf et al. [49], was used to validate the evaporation model. The initial droplet diameter was 0.526 mm and the free stream gas phase axial velocity and temperature was maintained at 3.2 m/s and 356 K, respectively. Fig. 1a shows the schematic of the flow domain for this validation. The flow was simulated on a 2D axisymmetric grid with the total number of grid points more than 36,000. The grid size in the vicinity of the droplet surface was approximately 15 μm × 6 μm. As the liquid is composed of one single component, the activation coefficient appearing in Eq. (8) is taken as unity. Similarly, the source terms due to interfacial mass transfer is suitably modified to account for single component evaporation.

Fig. 1b shows the comparison between experimental data and results from numerical simulation. The radius has been normalized with the initial droplet radius. The numerical results show an overall good agreement with the experimental results. At the later stages of droplet evolution, there is some deviation from the experimental results. Numerical simulation seems to be under predicting the droplet size, thereby indicating an over estimation of the interfacial mass transfer. The difference between experiment and the present validation test is about 2% at $t = 1$ s and later it increases to about 9% at $t = 2$ s. However, it should be noted that the error reported in [49] is about 3% for 1 mm diameter which subsequently increases for smaller diameter. As will be seen later, the flow time for all results that have been analysed in this study is less than 25 ms. Therefore, any deviation from the experimental results till $t = 1$ s is within the uncertainty limits of the experiment and hence acceptable for the present study. It must also be noted that the good agreement of numerical results with the experimental results justifies the assumption that the droplet interface is at thermodynamic equilibrium and the liquid/gas interface vapour mass fraction is equal to the saturated vapour mass fraction as determined by Eq. (8) for such droplet evaporation conditions.

Table 2
Thermo-physical properties of working fluids.

Properties	Data		
	Ethanol	Iso-octane	Air
T_C (K)	513.92	543.90	
Molecular weight	46.069	114.231	28.8
k Vapour (W/m K)	0.0154	0.0117	0.0242
k Liquid (W/m K)	0.182	0.0995	
μ Vapour (Pa s)	8.5753e-5	0.593e-5	1.789e-5
μ Liquid (Pa s)	1.233e-3	0.455e-3	
C_P vapour (J/kg K)	1006	1006	1006
C_P liquid (J/kg K)	2470	2037	
ρ liquid (kg/m^3)	813	695.5	

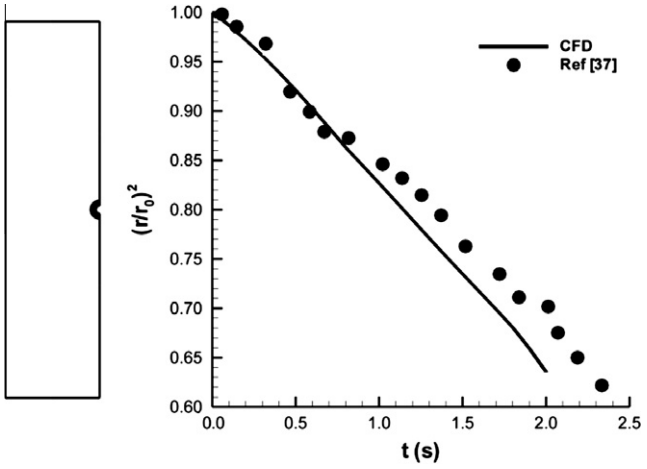

Fig. 1. (a) Schematic of the flow domain for validation case and (b) comparison of results from numerical and experimental data [37].

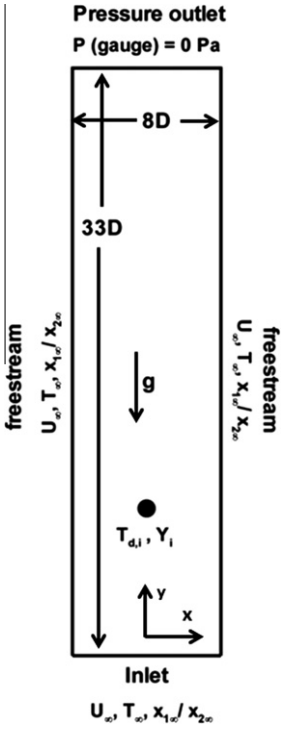

Fig. 2. Schematic of flow domain.

4. Results and discussion

A 2D flow domain, as shown in Fig. 2, was used to perform the simulations in this study. A single droplet composed of a binary mixture of ethanol and iso-octane was introduced in a stream of dry air which is at an elevated temperature. The flow domain is 8d in width and 33d in height, where d is the initial droplet

Table 3
Summary of grid independence study.

Grid	d/d_0	Evaporation rate (kg/s-m^3) $\times 10^{-6}$	$T_b/T_{b,i}$
40,000	0.993	42.03	1.0076
90,000	0.991	49.18	1.0063
160,000	0.990	58.04	1.0054
250,000	0.989	59.21	1.0048

diameter. The droplet was initially placed at a distance of 8d from the inlet. A base case was solved where the inlet free stream temperature and velocity is 400 K and 3.95 m/s, respectively. The droplet was initially at 300 K and its initial diameter was 300 μm, which corresponds approximately to a Reynolds number of 120. The initial mole fraction of ethanol in the droplet was 0.2, which may be considered as a surrogate for E20 blend of ethanol and gasoline. To determine the effect of various parameters on droplet evaporation, initial and boundary conditions were systematically changed and their effects were studied. The following parametric studies were performed:

- Set 1: Free stream temperature, $T_{g,\infty}$ (K) = 300, 325, 350 375, 400, 425, 450, 500, 550 and 600.
- Set 2: Free stream relative humidity of ethanol/iso-octane vapour, $x_{1,\infty}/x_{2,\infty}$ = 0/0, 0/0.25, 0/0.5, 0/0.75, 0.25/0, 0.5/0, 0.75/0, 0.25/0.75 and 0.75/0.25.
- Set 3: Droplet initial temperature, $T_{d,i}$ (K) = 280, 290, 300, 310, 320, 330, 340.
- Set 4: Initial droplet composition in terms of ethanol mole fraction, $X_{1,i}$ = 0, 0.1, 0.2, 0.5, 0.85 and 1.

Other than the parameter that was changed in each set, the remaining initial and boundary conditions were maintained same as in the base case. Unless otherwise stated, the liquid/gas interface was taken where the liquid volume fraction is 0.5. Relative humidity of ethanol or Iso-octane vapour is defined as the ratio of the vapour mole fraction in the free stream to the saturation mole fraction of that component at the given droplet temperature. A time step size of 1 μs was used in all the cases.

A grid independent study was performed to determine the optimum size of the grid elements. A uniform grid was initially created with 100 × 400 elements in x- and y-direction respectively. This grid was successively refined to create grids with 90,000, 160,000 and 250,000 grid elements. The base case was solved using these four grid configurations. Grid independence was determined by tabulating the droplet diameter, evaporation rate and droplet bulk temperature at t = 10.97 ms. Droplet diameter and bulk temperature were normalized by their initial values. The summary of grid independence study is given in Table 3. As can be seen from the table, when the number of grid elements is increased, the change in droplet diameter and bulk temperature between successive grid refinements is approximately 0.1%. However, the change in the evaporation rate between successive refinements is more significant. The change in evaporation rate is about 17% when the grid is refined from 40,000 to 90,000, about 18% when refined from 90,000 to 160,000 and about 2% when refined to 250,000. This difference between two successive grid refinements was considered to be acceptable for a grid independent solution. Therefore, grid with total number of elements of 250,000 was used in all the cases that were simulated in this study. x and y are equal to 10m with this grid density.

4.1. Base case

The droplet was initially at rest and therefore slip velocity, which is defined as the difference between the free stream velocity and droplet velocity, is same as the inlet free stream velocity magnitude. However, due to pressure and interfacial drag between the liquid and gas phases, the droplet is accelerated and it is displaced from its original position. The instantaneous droplet position and velocity at different times is given in Table 4. As can be seen from the table, the streamwise velocity magnitude continuous increases and therefore the streamwise slip velocity correspondingly decreases. This results in a decrease in the drag forces experienced by the droplet. In an earlier study [45] it was reported that the droplet deforms from its original cylindrical shape, which results in a higher surface to volume ratio. However, in this study the droplet retained its cylindrical shape throughout the length of its stay in the flow domain. This maybe because this study was performed at an initial droplet Re = 120, whereas the earlier study was performed at Re = 500. Hence, due to lower Reynolds number, the interphase shearing interaction was correspondingly lower and the droplet retained its original shape. It is also seen that the droplet has a slight left bias as it is displaced from its original position. This is because the droplet has a small transverse velocity component in the negative x-direction. The transverse velocity component is at least an order smaller than the streamwise velocity component.

Fig. 3 shows the gas phase contour plots of the relative velocity magnitude, streamtraces, temperature and ethanol mass fraction. Velocity is normalized as $|u - u_d|/U_\infty$; gas phase temperature as $(T - T_{d,i})/(T_\infty - T_{d,i})$; and vapour mass fraction as $y^i/y^i_{s,i}$. The peak relative velocity is about 20% higher than the inlet free stream velocity at t = 2.47 ms and subsequently it decreases to about the same magnitude as the inlet free stream velocity at t = 14.97 ms. This decrease in the velocity magnitude can be attributed to the fact that droplet is accelerating in the intermediate time period and the slip velocity between the gas phase and the liquid droplet correspondingly reduces. The streamtraces show that there is large recirculation bubble downstream of the droplet. There are two vortices in this region with each rotating in the opposite direction. However, the strength of each vortex is different as illustrated by their size. This gives the asymmetric nature of the wake region which in turn contributes to the transverse droplet velocity of the droplet in the negative x-direction. The asymmetry of the wake region maybe because the droplet Reynolds number is near the range where flow structures similar to Von Karman vortex shedding get initiated. Vortex shedding like structures has been reported earlier [45] for higher initial Reynolds number. The recirculation bubble extends to about 3 times the droplet diameter at t = 2.47 ms and then continuously reduces to about 0.5 times the droplet diameter at t = 14.97 ms. This can again be attributed to the decrease in the slip velocity. The gas phase temperature and vapour mass fraction is qualitatively similar with each showing a wake region downstream of the droplet. As expected, the gas phase temperature in the wake region of the droplet decreases with time whereas ethanol vapour mass fraction increases with time. The iso-octane vapour mass fraction profile will be qualitatively similar to the profile of ethanol vapour mass fraction.

Figs. 4–6 show the temporal evolution of streamwise velocity, temperature and ethanol mass fraction profiles along four horizontal planes downstream of the droplet at distances of y = 1d, 2d, 3d and 4d from the droplet centre. Tables 5a–d gives the

Table 4
Temporal evolution of droplet position and velocity for base case.

Time (ms)	x-Position ($\times d$)	y-Position ($\times d$)	x-Velocity (m/s)	y-Velocity (m/s)
2.47	0.003	8.75	−0.0017	0.097
4.97	0.034	10.09	−0.0047	0.199
10.97	0.256	16.39	−0.0167	0.401
14.97	0.425	23.74	−0.0054	0.657

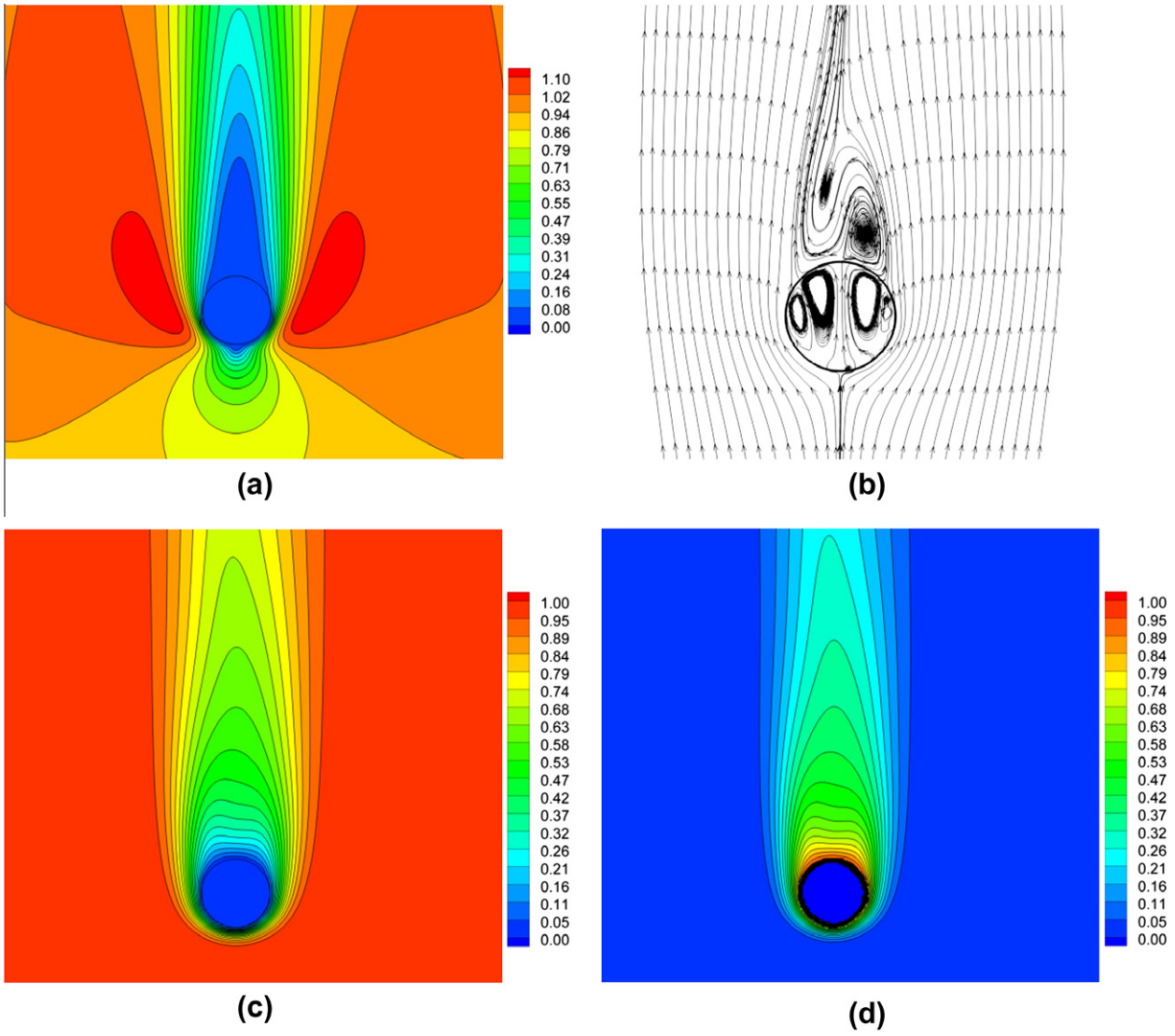

Fig. 3. Gas phase (a) $|u - u_d|/U_\infty$, (b) streamtraces, (c) $(T - T_{d,i})/(T_\infty - T_{d,i})$ and (d) $y^1/y^1_{s,i}$ for base case at $t = 10.97$ ms.

hydrodynamic, thermal and vapour wake thickness for the same four horizontal planes and flow times. As can be seen in the velocity plots, the minimum value in the wake region coincides with the longitudinal centre line of the flow domain for $t = 2.47$ ms and 4.97 ms. However, for $t = 10.97$ and 14.97 ms, the minimum values have shifted to the left because the droplet is also displaced transversely to the left hand side of the flow domain for these flow times. As expected, the hydrodynamic wake thickness generally increases with distance from the droplet as seen from the data in Table 5a. However, wake thickness also increases with time. This is because, as time increases, the slip velocity decreases and therefore the flow becomes more diffusion dominated, which in turn increases the momentum diffusion and hence hydrodynamic wake thickness increases with time. Negative values of streamwise velocity are seen at $y = 1$d for $t = 2.47$, 4.97 and 10.47 ms, indicating that this region is inside the recirculation bubble for these flow times. No negative values are seen at = 14.97 ms. Negative values of streamwise velocity stop appearing at $t = 10.47$ ms for $y = 2$d, $t = 4.97$ ms for $y = 3$d and $t = 2.47$ ms for $y = 4$d, thereby confirming the earlier observation from the streamtraces that the recirculation bubble is approximately 3 times the droplet diameter at $t = 2.47$ ms and it subsequently decreases.

The temperature in the wake region is lower than the free stream temperature due to heat transfer between the gas phase and the liquid droplet. The temperature in the wake region reduces with time for all the horizontal planes that are plotted in Fig. 5. The temperature at the intersection of the longitudinal centreline of the droplet and $y = 1$d decreases from 0.44 at $t = 2.47$ ms to 0.29 at $t = 14.97$ ms. Similar drop in temperature is also observed at other horizontal planes. As observed previously, the wake region shifts to the left with increasing flow time due to the transverse displacement of the droplet in the flow domain. When a horizontal plane is within the recirculation bubble, the gas phase temperature initially decreases along the radial distance on this plane. After traversing a certain distance from the longitudinal centreline, the temperature starts rising again till it reaches the free stream temperature. This profile can be observed for few planes in Fig. 5, for example, $y = 1$d and 2d for $t = 2.47$ and 4.97 ms. However, if the horizontal plane is outside the recirculation bubble, then the temperature monotonically increases as is observed for all flow times at $y = 4$d. Table 5b gives the thickness of thermal wake region and as observed from the data, the wake region thickness generally increases with distance and flow time. The thickness of the thermal wake region increases with distance as there is thermal diffusion in

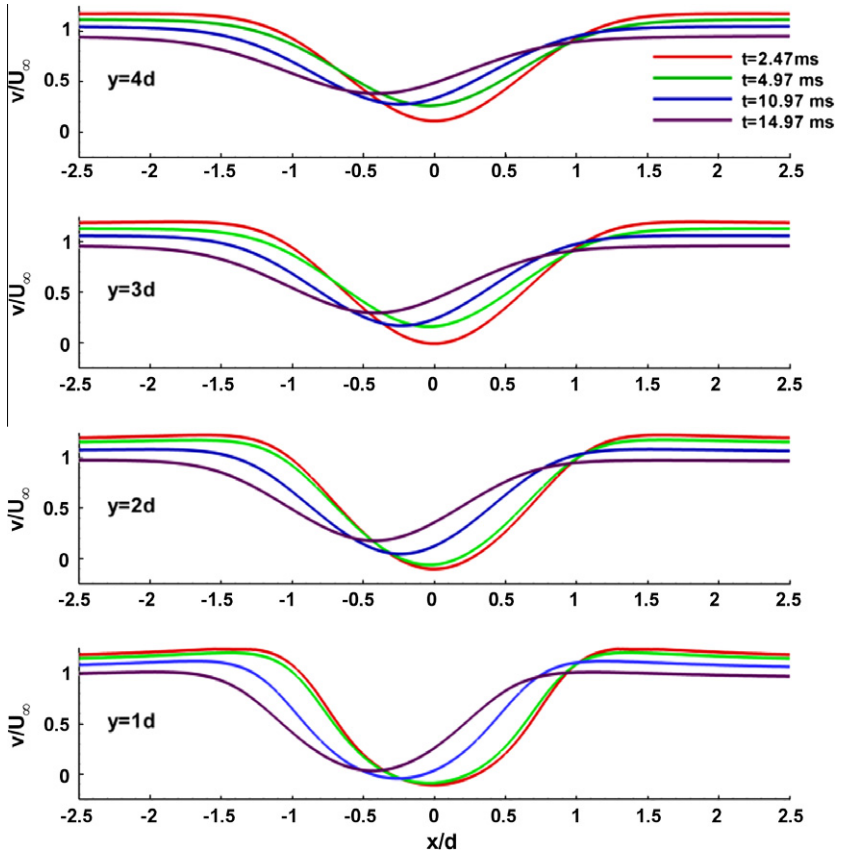

Fig. 4. Temporal evolution of normalized relative *y*-velocity component at *y* = 1d, 2d, 3d and 4d.

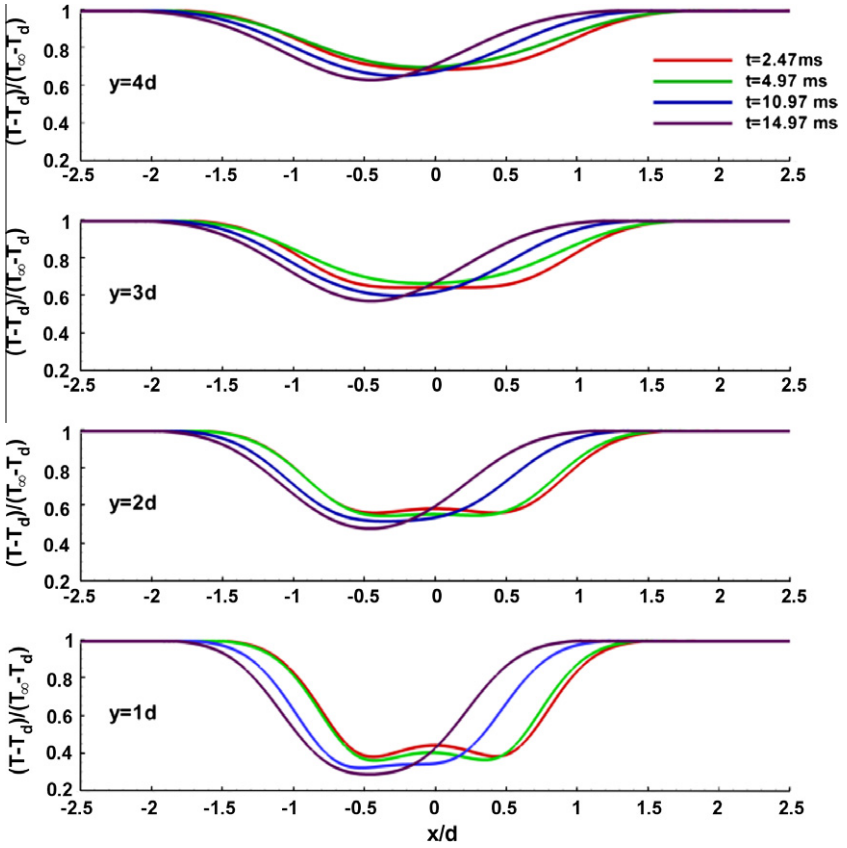

Fig. 5. Temporal evolution of normalized temperature at y = 1d, 2d, 3d and 4d.

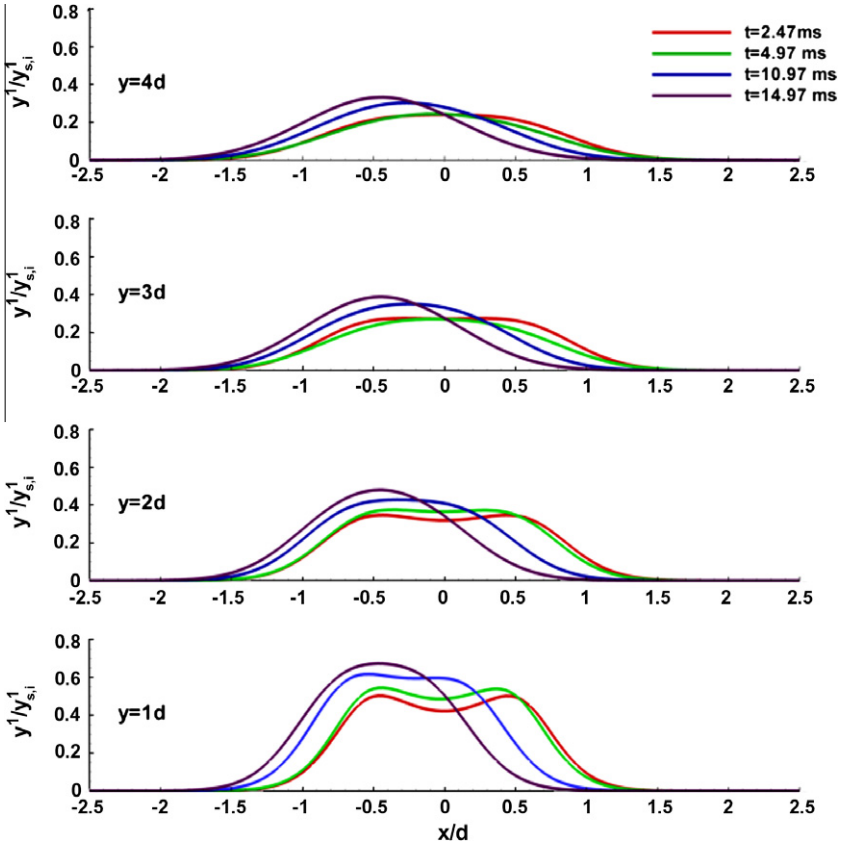

Fig. 6. Temporal evolution of normalized ethanol vapour mass fraction at y = 1d, 2d, 3d and 4d.

Table 5a
Hydrodynamic wake thickness.

	t = 2.47 ms	t = 4.97 ms	t = 10.97 ms	t = 14.97 ms
y = 1d	2.467	2.467	2.500	2.633
y = 2d	2.767	2.833	2.933	3.267
y = 3d	3.000	3.433	3.367	3.533
y = 4d	3.267	3.800	3.767	4.533

Table 5b
Thermal wake thickness.

	t = 2.47 ms	t = 4.97 ms	t = 10.97 ms	t = 14.97 ms
y = 1d	3.000	2.933	2.867	2.800
y = 2d	3.367	3.333	3.233	3.133
y = 3d	3.600	3.733	3.467	3.367
y = 4d	3.800	3.933	3.700	3.600

Table 5c
Ethanol vapour wake thickness.

	t = 2.47 ms	t = 4.97 ms	t = 10.97 ms	t = 14.97 ms
y = 1d	2.800	2.733	2.667	2.567
y = 2d	3.133	3.067	2.967	2.833
y = 3d	3.333	3.433	3.133	3.033
y = 4d	3.500	3.567	3.333	3.233

Table 5d
Iso-octane vapour wake thickness.

	t = 2.47 ms	t = 4.97 ms	t = 10.97 ms	t = 14.97 ms
y = 1d	2.467	2.400	2.333	2.200
y = 2d	2.733	2.667	2.200	2.333
y = 3d	2.867	2.833	2.600	2.433
y = 4d	2.933	2.900	2.667	2.567

the radial direction due to sensible heat transfer. Also, the thermal wake thickness increases with time because as the slip velocity decreases, the flow becomes more diffusion dominated. It should also be noted that the thermal wake is thicker than the hydrodynamic wake because Prandtl number is less than unity. However, for few horizontal planes and flow times, the thermal wake is thinner than the hydrodynamic wake even though Prandtl number is less than unity. This may be because at this time the droplet is offset towards the left boundary and therefore the left boundary condition will have a larger influence on the flow field. As a result of this influence, the thermal wake is forced to become thinner and this is increasingly felt away from the droplet.

In case of ethanol vapour mass fraction, the maximum vapour mass fraction is in the wake region and it decreases in the radial direction. Similar to the observation made for the temperature profile, when the horizontal plane is within the recirculation bubble, the vapour mass fraction initially increases till a certain radial distance before decreasing to the free stream value, which in this case is zero. As before, this profile is clearly observed for y = 1d and 2d at t = 2.47 ms and 4.97 ms in Fig. 6. For horizontal planes which are outside the recirculation bubble, the vapour mass fraction monotonically decreases to zero. This is observed for all flow times at y = 4d. As observed before, the wake region for t = 10.97 and 14.97 ms is offset to the left as the droplet is also transversely offset. Tables 5c and d gives the values of wake thickness of ethanol and iso-octane vapours, respectively. In a pattern similar to the hydrodynamic and thermal wake thickness, the vapour wake thicknesses generally increases with time and distance from the

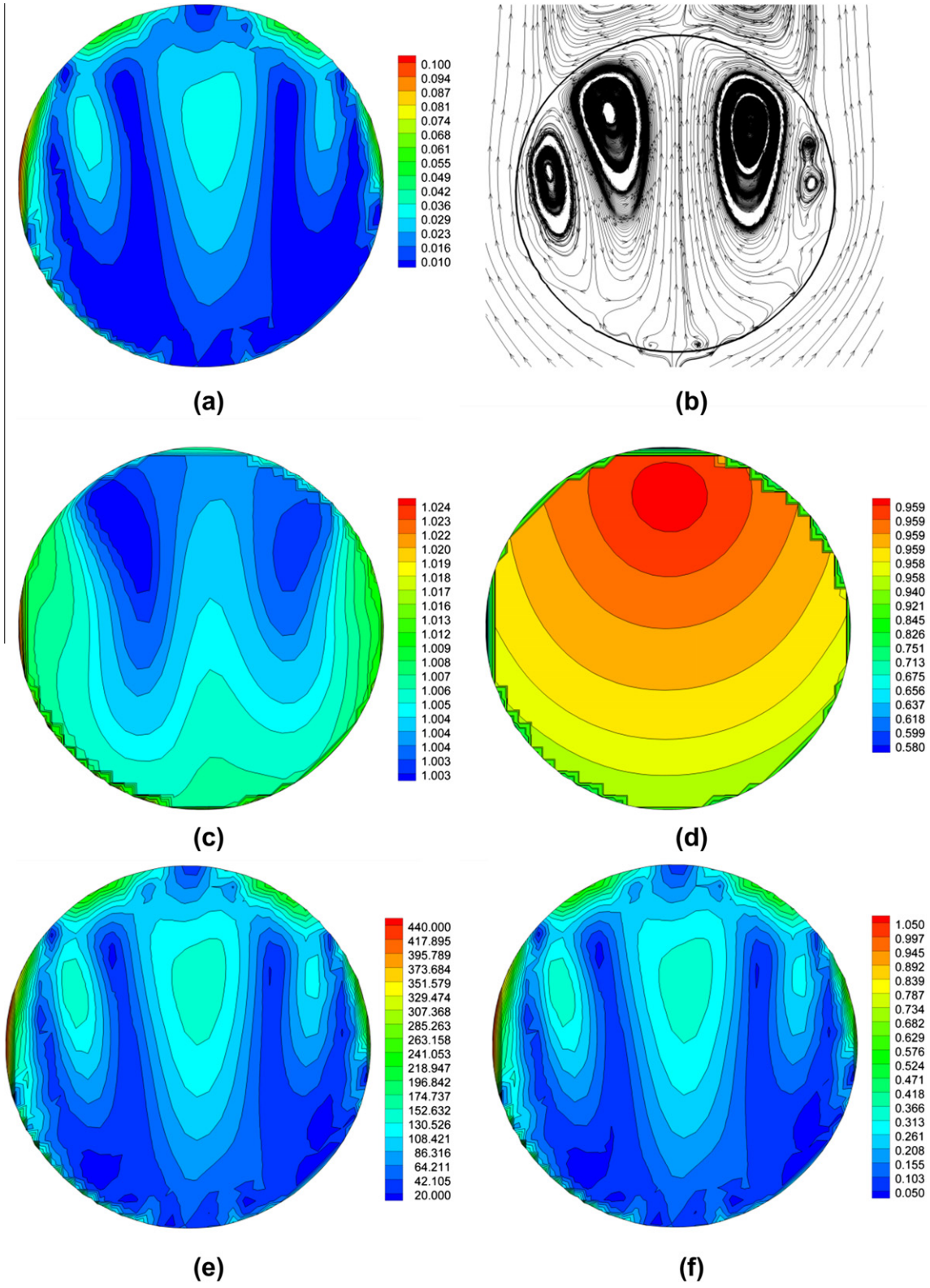

Fig. 7. Gas phase (a) $|u - u_d|/U_\infty$, (b) streamtraces, (c) $T/T_{d,i}$, (d) $Y/Y_{d,i}$, (e) thermal Pe No. and (f) species Pe No. for base case at $t = 10.97$ ms.

droplet. Ethanol vapour wake thickness is generally thicker than hydrodynamic wake thickness indicating that Schmidt number for ethanol vapour is lower than unity. However, the wake thickness of iso-octane vapour is always thinner than hydrodynamic wake thickness. This is because iso-octane is a larger molecule compared to ethanol and therefore its vapour diffuses slowly in the gas phase. Hence its Schmidt number is always greater than unity. As before, the influence of the left boundary seem to have a greater impact for species wake thickness for $t = 14.97$ ms due to the left offset of the droplet in the flow domain. It should be noted that the hydrodynamic, thermal and species wake thickness break their respective trend for $y = 3d$ and $4d$ at $t = 4.97$ ms.

This is most probably because the droplet is offset to the left at later times and therefore the side boundaries maybe marginally influencing the free growth of the wake region.

Fig. 7 shows the fluid flow characteristics inside the liquid droplet. The definition of relative velocity in the liquid phase is same as in gas phase. However, temperature and ethanol mass fraction is normalized as $T/T_{d,i}$ and $Y/Y_{d,i}$, where $T_{d,i}$ and $Y_{d,i}$ are the initial droplet temperature and ethanol mass fraction respectively. Due to the shearing interaction with the gas phase, recirculation vortices are seen inside the droplet. The velocity magnitude of these convective currents is small compared to the free stream velocity. The area weighted average of the convective currents increases from about 1.3% of the free stream velocity magnitude at $t = 2.47$ ms to about 2.1 % at $t = 14.97$ ms. The size and shape of these vortices change with time. Initially, the shape and size of the vortices are symmetrical about the longitudinal centre line of the droplet. However, at later times, the vortices become asymmetrical about the droplet centre line. Due to the asymmetrical nature of the wake region in the gas phase, there is a difference in the shear stress profile on the left and right hand side of the droplet interface, which in turn maybe creating the asymmetric vortex pattern in the droplet interior. The temperature profile within the droplet follows the convection currents. However, this is not the case for ethanol mass fraction profile. As can be seen from the figure, ethanol mass fraction is diffusion dominated and the highest values appear near the rear end of the droplet. This difference in the thermal and species profile can be explained by analysing the thermal and species Peclet number. As can be seen in Fig. 7, thermal Peclet number is about two orders larger than the species Peclet number. Small values of Peclet number indicate that the species profile is diffusion dominated. There is a steady increase in the droplet bulk temperature, where bulk temperature is defined as, $T_b = \int_{V_{fluid}} \alpha_l \rho_l Cp_l T dV / \int_{V_{fluid}} \alpha_l \rho_l Cp_l dV$. The bulk temperature of the droplet increases by approximately 0.7% from its initial temperature after 14.97 ms. As the evaporation rate of ethanol in terms of number of moles per unit time is higher than that of iso-octane, droplet becomes leaner in ethanol with time. The mass fraction of ethanol in droplet reduces by approximately 6% from its initial value after 14.97 ms.

Fig. 8 shows the temperature, ethanol and iso-octane vapour mass fraction, liquid ethanol mass fraction, total evaporation rate and latent heat transfer distribution along the droplet interface at $t = 10.97$ ms. As mentioned before, droplet interface is defined along an iso-surface where liquid volume fraction is 0.5. The droplet interface is further subdivided into the front and rear halves to analyse the effect of free stream and wake region on the distribution of the above mentioned parameters. As the front half of the droplet is exposed to the free stream temperature, which is the highest in the flow domain, the interface temperature in the front half of the droplet is higher than the rear half of the droplet. The temperature increases towards the side for both the front and rear halves. However, at other times, the highest temperature is seen more towards the central portion of the front half and lower at the sides. This changing pattern of the temperature profile may be because of the changing nature of the internal circulation within the droplet and also because the slip velocity between the gas phase and the droplet reduces with time which in turn changes the flow separation point along the droplet surface. Ethanol and iso-octane vapour mass fraction is lowest along the front half of the droplet because the free stream relative humidity is zero.

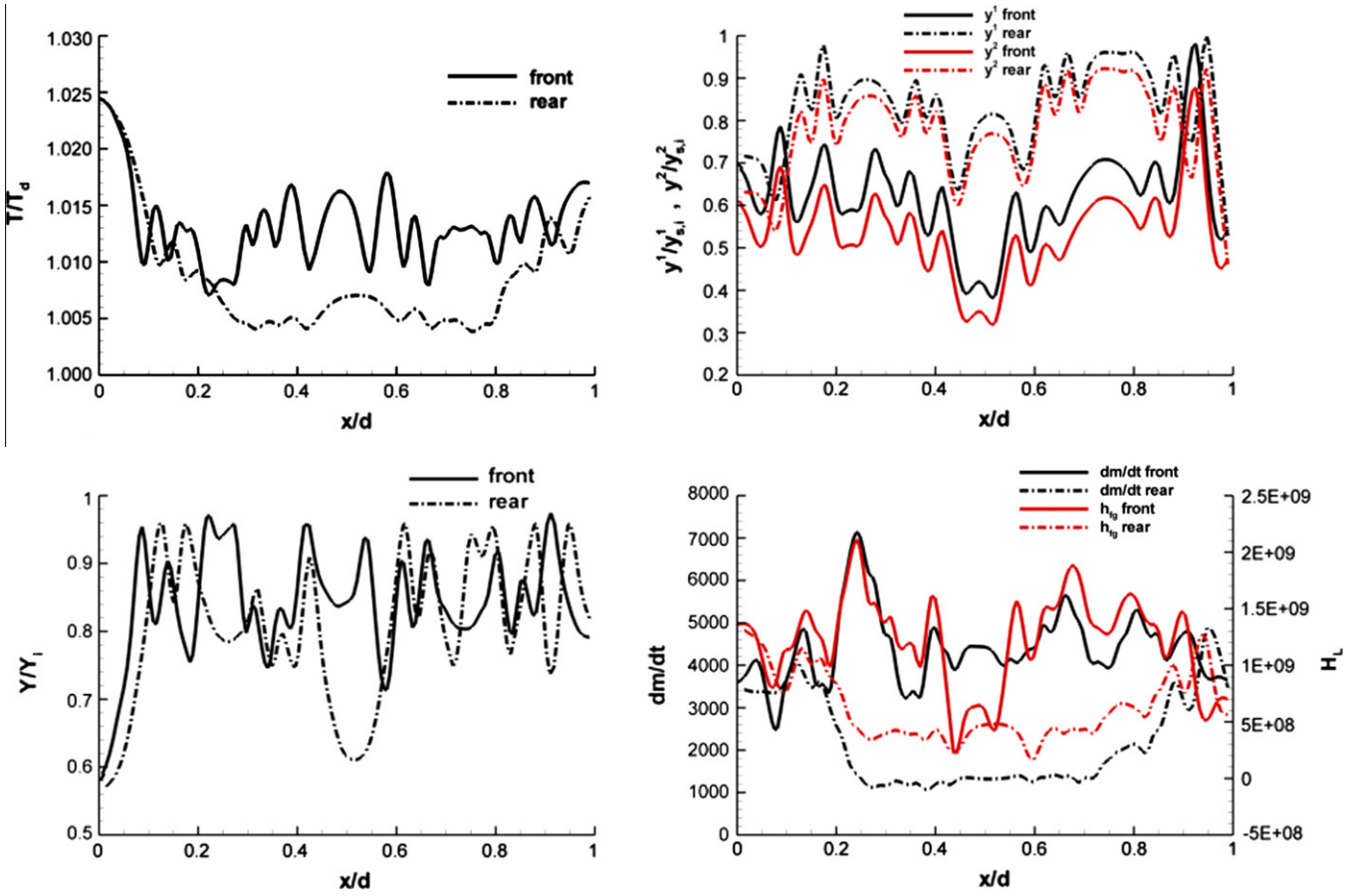

Fig. 8. Interfacial values of normalized temperature, normalized ethanol and iso-octane vapour mass fraction, normalized liquid ethanol mass fraction, total evaporation rate and total latent heat transfer.

However, due to evaporation, vapour mass fraction is higher in the rear half of the droplet. No significant difference is seen between the front and rear halves of the droplet interface profile of liquid ethanol mass fraction. The evaporation rate and consequently the latent heat of evaporation are markedly higher in the front half of the droplet than in the rear half. This is expected because as the free stream vapour mass fraction is zero, the mass fraction gradient at the droplet interface is higher in the front half. As the wake region has significantly higher vapour, the mass fraction gradient in the rear half is lower. This results in a significantly higher evaporation rate in the front half. Hence, latent heat transfer is also higher in this region. The evaporation rate is lower in the rear half of the droplet and consequently, latent heat transfer also decreases.

4.2. Parametric study

Fig. 9 shows the results from simulation set 1, where the free stream temperature is increased from 300 K to 600 K. Temporal evolution of evaporation rate and droplet diameter, bulk temperature and ethanol mass fraction is plotted. When free stream temperature is 300 K, the droplet and the gas phase are initially at the same temperature and therefore there is no sensible heat transfer between the droplet and the gas phase. Interfacial mass transfer takes place due to the difference in vapour mass fraction at the droplet surface and free stream. However, due to absence of sensible heat transfer from the gas phase, the droplet bulk temperature reduces with time due to evaporative cooling. This in turn reduces the vapour pressure at the liquid/gas interface and consequently, the evaporation rate decreases with time. However, as the free stream temperature increases, sensible heat transfer from the gas phase increases and therefore, influence of latent heat transfer reduces. When $T_{g,}$ = 400 K, the evaporation rate is almost constant with time, though there is slight upward bias for droplet bulk temperature, indicating that latent heat transfer is almost balanced with sensible heat transfer and therefore the droplet temperature does not change significantly with time. However, at higher temperatures, sensible heat transfer predominates over latent heat transfer and therefore, the droplet bulk temperature increases more appreciably. However, when the droplet bulk temperature increases, vapour pressure also increases which in turn increases the evaporation rate. Hence evaporation rate at $T_{g,}$ = 600 K is highest among all the cases studied in this simulation set. There is steady decrease in the droplet diameter and ethanol mass fraction in the droplet. Due to evaporation, the droplet volume decreases and therefore there is a corresponding decrease in droplet diameter. Also, evaporation rate in terms of number of moles per unit time is higher for ethanol as compared to iso-octane because the partial pressure of ethanol is higher in this mixture. Hence the droplet becomes leaner in ethanol.

When the free stream composition is changed, the difference between the saturation mass fraction at the liquid/gas interface and the free stream changes. This in turn changes the magnitude of vapour mass fraction gradient in Eq. (7). This effect of free stream vapour composition on temporal evolution of the droplet is shown in Fig. 10. In this plot, the evaporation rate of ethanol and iso-octane is plotted separately along with the total evaporation rate. As can be seen from the evaporation rate plots, the evaporation of ethanol or iso-octane is depressed when the relative humidity of that particular species is increased in the free stream. This is because the vapour mass fraction gradient of that particular species decreases when its mass fraction in the free stream is increased. The evaporation rate of ethanol is very similar for the cases where x_1/x_2 = 0/0, 0/0.25, 0/0.5, 0/0.75. Similarly, the

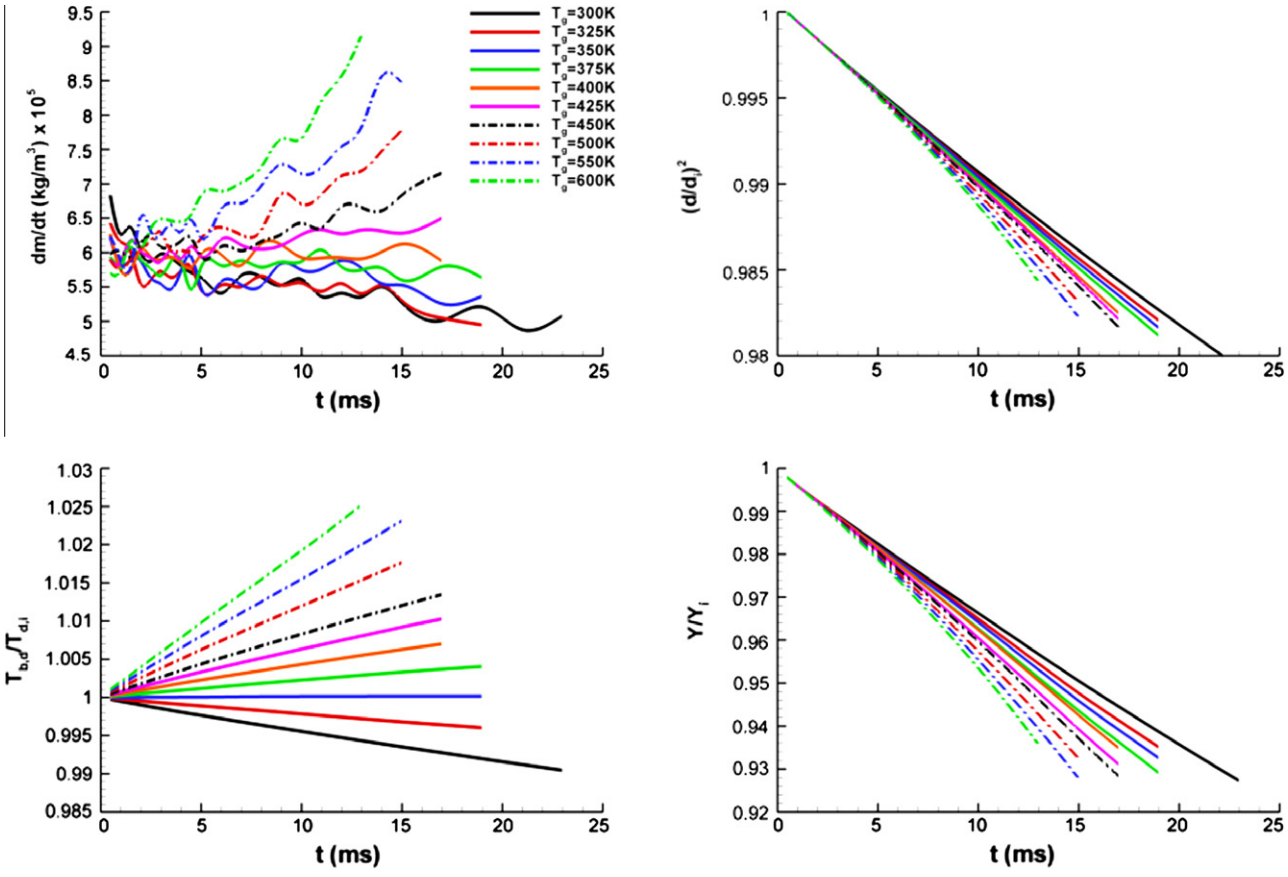

Fig. 9. Temporal evolution of evaporation rate, droplet diameter, droplet bulk temperature and droplet ethanol mass fraction with increasing free stream temperature.

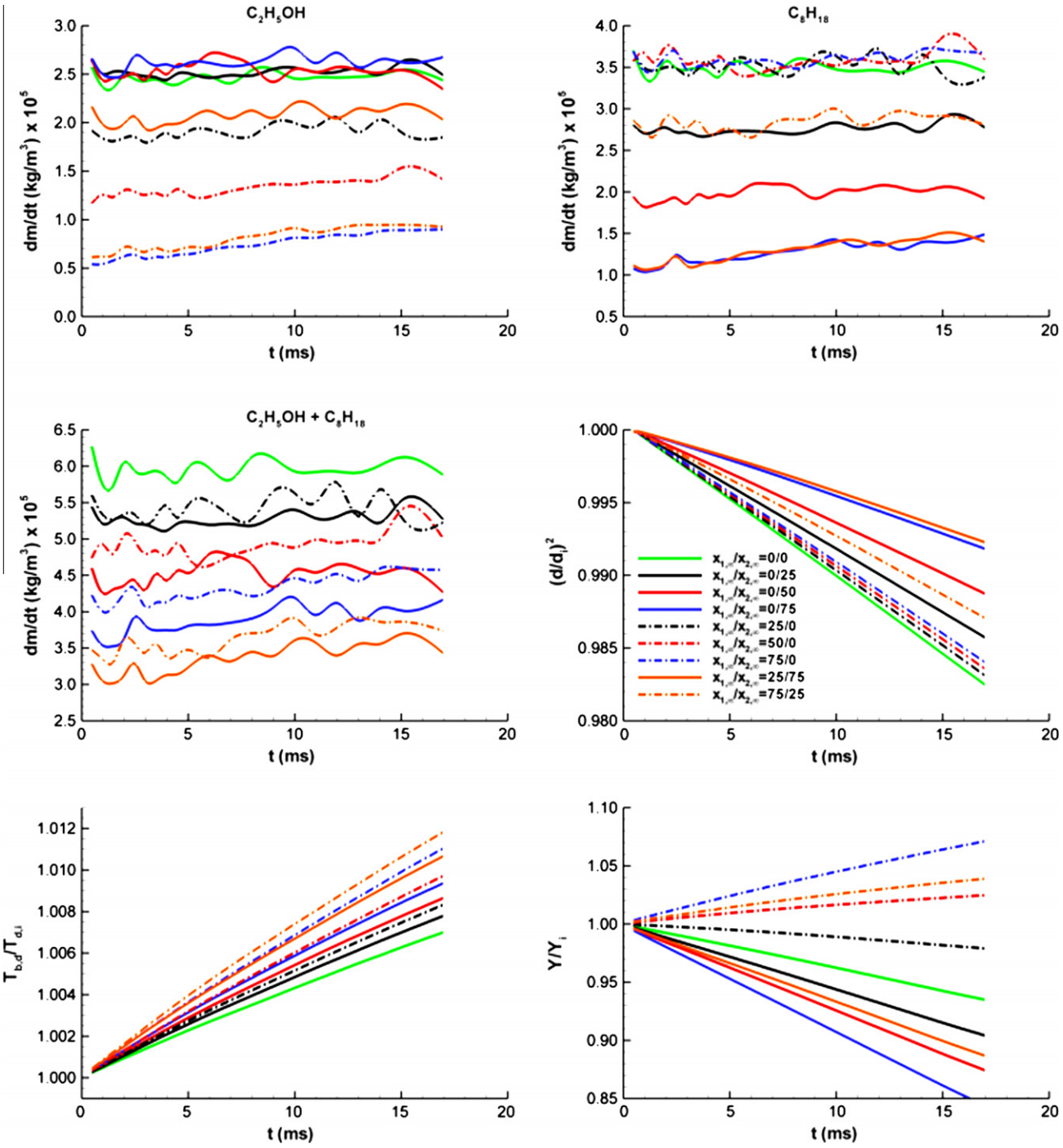

Fig. 10. Temporal evolution of ethanol and iso-octane evaporation rate, droplet diameter, droplet bulk temperature and droplet ethanol mass fraction with varying free stream vapour composition.

evaporation of iso-octane is very similar for the cases where x_1/x_2 = 0/0, 0.25/0, 0.5/0, 0.75/0. This implies that evaporation rate of one species is not strongly influenced by the free stream mass fraction of the other species. However, when total evaporation rate is analysed, it is seen that there is a steady decrease in the evaporation rate when the vapour relative humidity is increased. Also for similar magnitude of relative humidity, the total evaporation rate is higher for cases where the gas phase is loaded with ethanol vapour as compared to cases where the gas phases is loaded with iso-octane vapour. For example, total evaporation rate of x_1/x_2 = 0.25/0 is higher than x_1/x_2 = 0/0.25. This is because; the molecular weight of iso-octane is larger than the molecular weight of ethanol. Therefore, even though the evaporation rate of iso-octane in terms number of moles per unit time is lower, evaporation rate in terms of mass per unit time is higher. Droplet diameter is least for x_1/x_2 = 0/0 because evaporation rate was highest for this case. Droplet diameter is less for cases where the gas phase is loaded with ethanol compared to cases where the gas phase was loaded with iso-octane for similar magnitude of relative humidity. This is because, when evaporation rate is same, the decrease in droplet volume would be higher for cases where there is higher evaporation of iso-octane as liquid iso-octane has lower density. Therefore, for example, droplet diameter is lower for x_1/x_2 = 0.25/0 than when x_1/x_2 = 0/0.25. Droplet bulk temperature rises with time due to sensible heating from the gas phase. However this rise in bulk temperature is influenced by two factors: (a) latent heat transfer and

(b) liquid composition. Latent heat of evaporation for ethanol is higher than that of iso-octane. Therefore, evaporative cooling due to latent heat transfer will be stronger for cases when relative humidity of iso-octane is increased in the free-stream compared to the cases where relative humidity of ethanol is increased. Bulk temperature of the droplet, by definition, depends on heat capacitance which is defined as the product of density and specific heat. From the thermo-physical properties given in Table 2, it can be seen that the heat capacitance of ethanol is higher than iso-octane. For given amount of sensible heating, fluid with higher heat capacitance will result in lower temperature rise. Hence the overall rise in droplet temperature will depend on the interplay of these two factors. As can be seen from Fig. 10, the bulk temperature is lowest when the relative humidity of both ethanol and iso-octane is zero in the free stream. This is because evaporation rate is highest in this case and therefore latent heat transfer predominates over the influence of sensible heat transfer. When the relative humidity is increased, the bulk temperature of the droplet also increases. However, the increase in droplet bulk temperature does not always follow the trend seen in evaporation rate. Examples of such differences are:

(i) total evaporation rate of 0.75/0 case is higher than 0/0.75. However, evaporation rate of ethanol is significantly higher for 0/0.75 as compared to 0.75/0. Therefore latent heat transfer is higher for the case 0/0.75. Droplet becomes increasingly leaner in ethanol for the case 0/0.75 which in turn reduces its heat capacitance and therefore there should be a higher temperature rise due to sensible heating. As the droplet temperature for 0/0.75 case is lower than 0.75/0, this indicates that the influence of latent heat is stronger than the influence of sensible heating.

(ii) a similar observation can also be made between 0.75/0 and 0.25/0.75. Even though the total evaporation rate of 0.75/0 is higher than 0.25/0.75 by about 30%, droplet bulk temperature of the later is lower. However, the temperature difference between the two cases is less due to the smaller difference in the ethanol evaporation rate.

The droplet becomes increasingly leaner in ethanol for cases where evaporation of iso-octane is depressed due to high relative humidity of iso-octane vapour in free stream. The droplet still becomes leaner for 0/0 and 0.25/0 cases. However, for other cases, where ethanol evaporation is depressed due to high relative humidity of ethanol vapour, the droplet becomes richer in ethanol with increase in flow time.

Initial droplet temperature is varied in simulation set 3 and the results from that set is plotted in Fig. 11. Initial droplet temperature has a very strong influence on evaporation rate. As the liquid temperature is raised, the evaporation rate correspondingly increases. The evaporation rate increases by approximately 680% when droplet temperature is raised from 280 K to 340 K. This can be attributed to the fact that vapour pressure is a strong function of liquid temperature which in turn affects the saturation vapour mass fraction at the liquid/gas interface. The droplet diameter monotonically decreases with time and the rate of decrease increases with temperature. This directly corresponds to the increase in evaporation rate. The diameter decreases by about 4% at $T_{d,i}$ = 340 K, which is the highest among all the cases simulated in this study. As the droplet size becomes increasingly smaller, the drag forces become larger than the weight of the droplet which in turn accelerates the droplet at a faster rate. Therefore, the droplet is displaced from the flow domain within a shorter period of

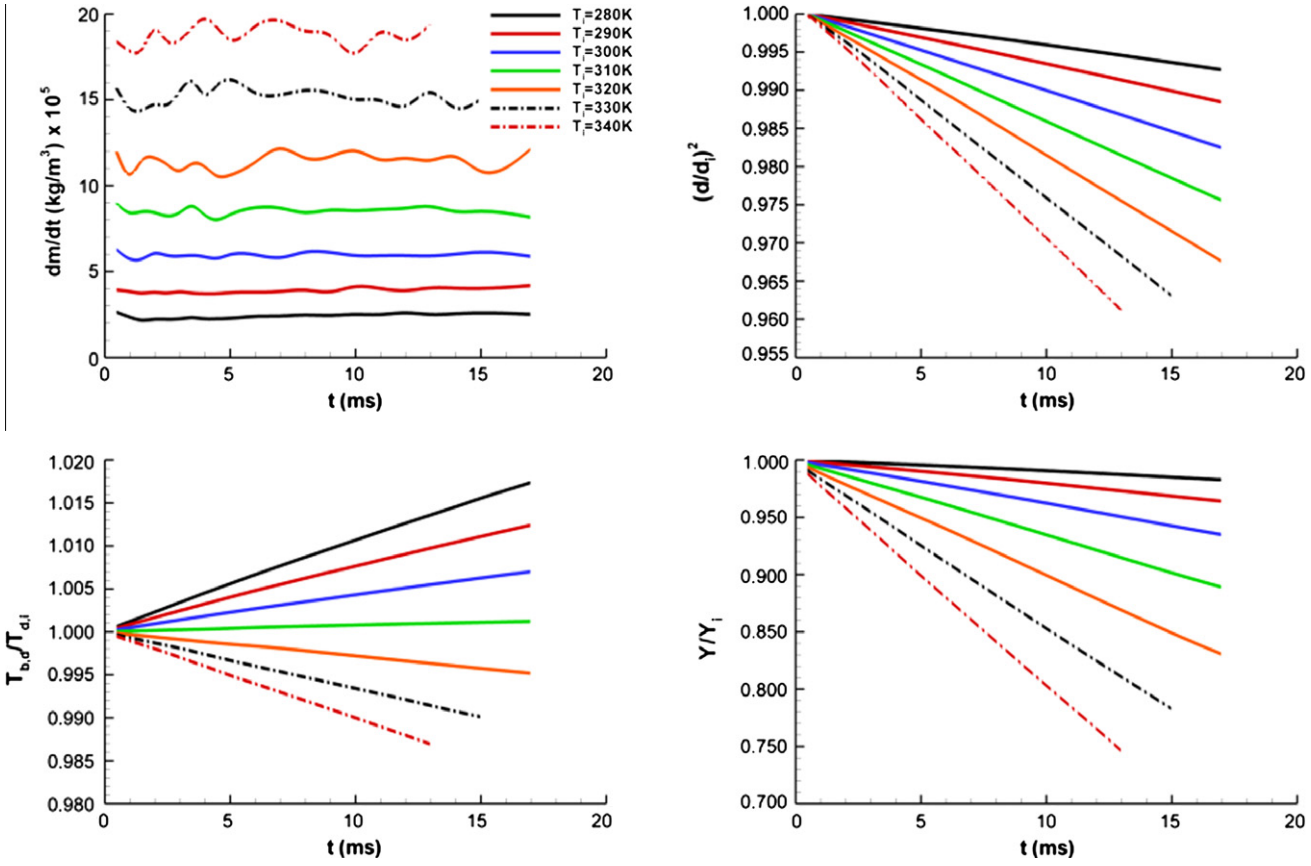

Fig. 11. Temporal evolution of evaporation rate, droplet diameter, droplet bulk temperature and droplet ethanol mass fraction with increasing droplet temperature.

time when initial droplet temperature is increased. Hence, the case $T_{d,i}$ = 340 K was analysed till 12.97 ms as compared to $T_{d,i}$ = 300 K, which was analysed till 16.97 ms. When the initial droplet temperature is lower, the droplet bulk temperature increases with time due to sensible heating. However, at higher initial temperatures, the evaporation rate is higher and therefore latent heat transfer becomes more significant. Hence, the droplet bulk temperature decreases for the cases $T_{d,i}$ = 320 K, 330 K and 340 K. Similarly, due to higher evaporation rate at higher droplet temperatures, the droplet becomes increasingly leaner in ethanol. Therefore, at t = 12.97 ms, ethanol mass fraction reduces by 25% when $T_{d,i}$ = 340 K as compared to about 1% when $T_{d,i}$ = 280 K.

In the final simulation set, ethanol mole fraction in the droplet was varied from 0 to 1 and results are plotted in Fig. 12. Evaporation rate for the cases X_i = 0.1, 0.2 and 0.5 are very close because the vapour pressure for these three liquid composition is very similar. However, as vapour pressure is slightly lower when X_i = 0.85, the evaporation rate is correspondingly lower. When X_i = 0 and 1, the evaporation rates are significantly lower because the vapour pressure of the pure fluids are also significantly lower than when they are in mixture. The size of the droplet reduces for all the case with time due to interfacial mass transfer. In a similar argument forwarded before, for the same evaporation rate, the diameter of the droplet with higher iso-octane content will reduce more because, as can be seen in Table 2, liquid iso-octane has a lower density than ethanol. However, contrary to the above argument, it can be seen from Fig. 12 that the case X_i = 0.5 has the smallest diameter at t = 16.97 ms among the cases X_i = 0.1, 0.2 and 0.5, even though the total evaporation rate for all the three cases are approximately the same. However, when a time integration of the evaporation rate of individual component is performed, it was found that overall mass evaporated was least when X_i = 0.1. The total mass evaporated for X_i = 0.2 and 0.5 is almost equal, however, time integration of interfacial mass transfer for iso-octane for X_i = 0.5 was marginally higher than that of X_i = 0.2. This is because saturation mass fraction of iso-octane vapour for X_i = 0.5 is higher than that of X_i = 0.2. X_i = 1 shows the largest droplet at t = 16.97 ms as its evaporation rate is the lowest. Temperature rise for X_i = 0 is the highest because of its lower latent heat of evaporation and therefore the effect of sensible heat is higher. As noted before, heat capacitance of iso-octane is lower than that of ethanol. This also contributed to its higher droplet temperature. A similar argument can also be made to explain why X_i = 0.85 has the least temperature even though its evaporation rate is slightly lower than X_i = 0.1, 0.2 and 0.5. Due to its higher ethanol content, it takes a higher amount of sensible heat to increase the droplet temperature. Hence, the slightly lower latent cooling is compensated by its higher heat capacitance and hence its temperature is lowest among all the cases. Droplet bulk temperature rises with decrease in ethanol content. Also, bulk temperature for X_i = 1 is very similar to X_i = 0.2, even though its evaporation rate was the least. This is because heat capacitance is highest for X_i = 1. Droplet ethanol mass fraction was plotted only for the cases X_i = 0.1, 0.2. 0.5 and 0.85. Results for X_i = 0 and 1 are not plotted as they are trivial in nature. As can be seen from the plot, droplet ethanol content increases with increase in initial ethanol content. Hence, the droplet is leanest for X_i = 0.1; there is no change in liquid ethanol mass fraction for X_i = 0.5; and the droplet becomes richer in ethanol when X_i = 0.85.

5. Conclusions

Evaporation from the surface of a single droplet composed of ethanol and iso-octane was numerically studied. VOF

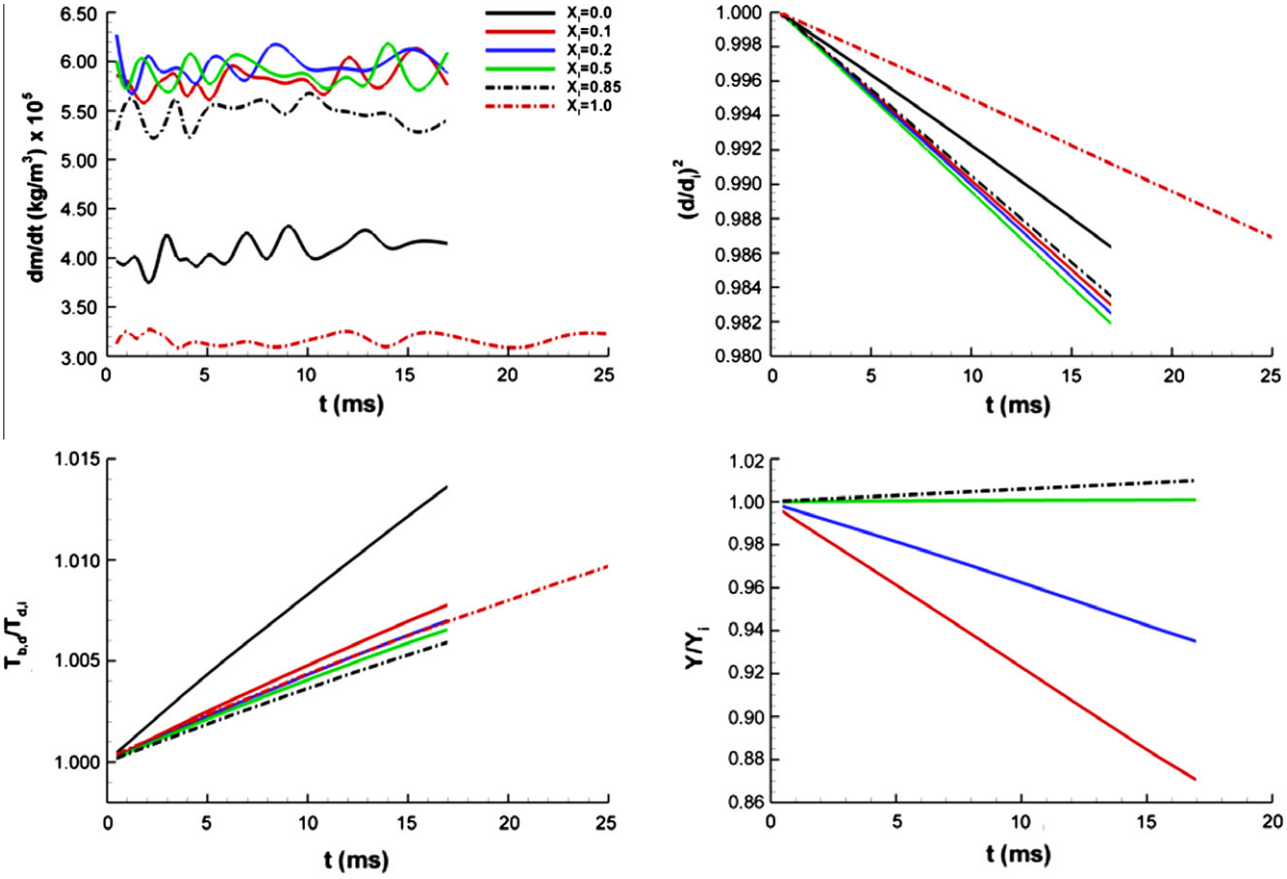

Fig. 12. Temporal evolution of evaporation rate, droplet diameter, droplet bulk temperature and droplet ethanol mass fraction with increasing ethanol content in droplet.

multiphase model was used to track the liquid gas interface. Effect of ambient air temperature, air composition, liquid temperature and liquid composition on droplet evaporation was studied. Some of the major observations from this study are:

- Internal convection currents are initiated within the droplet due to shearing interaction between the liquid and gas phases. These convection currents affect the temperature distribution. As the species Peclet number was small, internal convection currents did not affect the species distribution within the droplet.
- The wake region of the droplet is asymmetrical and therefore the droplet is subjected to lateral displacement within the flow domain.
- Droplet temperature seems to have the most significant effect on evaporation rate. With the increase in droplet temperature there is a significant rise in evaporation rate.
- There is a strong interplay between droplet composition and the species that is predominantly evaporating because droplet composition affects heat capacitance which in turn affect temperature rise due to sensible heat transfer and predominant evaporating species affects latent heat transfer. Therefore, overall droplet temperature is dependent on the relative strength of sensible and latent heat transfer.
- Droplet composition also affects the change in droplet size because overall volume change in dependent on the evaporation rate of the individual components which is in turn depends on the partial pressure of the individual components in the gas phase.

Acknowledgments

The author would like to acknowledge support of Indian Institute of Technology Hyderabad for providing access to computer hardware and software used in this work. Author would also like to thank Raja Gopinath for providing for assistance in validating the evaporation model.

References

[1] Lefebvre AH. Atomization and sprays. Boca Raton, FL: CRC Press; 1989.
[2] Agarwal AK. Biofuels (alcohols and biodiesel) applications as fuels for internal combustion engines. Prog Energy Combust Sci 2007;33:233–71.
[3] Drake MC, Haworth DC. Advanced gasoline engine development using optical diagnostics and numerical modelling. Proc Combust Inst 2007;31:99–124.
[4] Jiang X, Siamas GA, Jagus K, Karayiannis TG. Physical modelling and advanced simulations of gas–liquid two-phase jet flows in atomization and sprays. Prog Energy Combust Sci 2010;36:131–67.
[5] Godsave GA. Studies of the combustion of drops in a fuel spray - the burning of single drops of fuel. In: 4th International symposium on combustion. Baltimore: The Combustion Institute; 1953. p. 818–30.
[6] Spalding DB. The combustion of liquid fuels. In: 4th International symposium on combustion. Baltimore: The Combustion Institute; 1953. p. 847–64.
[7] Law CK. Unsteady droplet combustion with droplet heating. Combust Flame 1976;26:17–22.
[8] Sirignano WA, Law CK. Unsteady droplet combustion and droplet heating-ii: conduction limit. Combust Flame 1977;28:175–86.
[9] Sirignano WA, Law CK. Transient heat and liquid phase mass diffusion in fuel droplet vaporization. In: Zung, editor. Evaporation–combustion of fuels, Washington, DC: American Society of Chemical Society; 1978, p. 3–26.
[10] Haywood RJ, Nafziger R, Renksizbulut M. A detailed examination of gas and liquid phase transient processes in convective droplet evaporation. J Heat Transfer 1989;111:495–502.
[11] Haywood RJ, Renksizbulut M, Raithby GD. Transient deformation and evaporation of droplets at intermediate Reynolds numbers. Int J Heat Mass Transfer 1994;37:1401–9.
[12] Miller RS, Harstad K, Bellan J. Evaluation of equilibrium and non-equilibrium evaporation models for many-droplet gas–liquid flow simulations. Int J Multiphase Flow 1998;24:1025–55.
[13] Abarham M, Wichman IS. Mono-component fuel droplet evaporation in the presence of background fuel vapour. Int J Heat Mass Transfer 2011;54:4090–8.
[14] Bhattacharya P, Ghosal S, Som SK. Evaporation of multicomponent liquid fuel droplets. Int J Energy Res 1996;20:385–98.
[15] Sezen Y. Unsteady mass transfer analysis of evaporation of a single multicomponent droplet with diffusion and constant rate processes. Int Commun Heat Mass Transfer 2000;27:559–68.
[16] Nadykto AB, Schukin ER, Kulmala M, Laaksonen A. Evaporation and condensation rates of a multicomponent droplet in a non-isothermal gas mixture. J Aerosol Sci 2000;31:S801–2.
[17] Zeng Y, Lee C-fon. Multicomponent-fuel film-vaporization model for multidimensional computations. J Propul Power 2000;16:964–73.
[18] Yao G. A film-theory-based model for a multicomponent droplet evaporation at both low- and high-pressure environments. J Heat Transfer 2006;128:290–4.
[19] Sazhin SS, Elwardany A, Krutitskii PA, Castanet G, Lemoine F, Sazhina EM, et al. A simplified model for bi-component droplet heating and evaporation. Int J Heat Mass Transfer 2010;53:4495–505.
[20] Sazhin SS, Elwardany A, Krutitskii PA, Deprédurand V, Castanet G, Lemoine F, et al. Multi-component droplet heating and evaporation: numerical simulation versus experimental data. Int J Therm Sci 2011;50:1164–80.
[21] Sazhin SS, Elwardany AE, Sazhina EM, Heikal MR. A quasi-discrete model for heating and evaporation of complex multicomponent hydrocarbon fuel droplets. Int J Heat Mass Transfer 2011;54:4325–32.
[22] Aggarwal SK, Mongia HC. Multicomponent and high-pressure effects on droplet vaporization. J Eng Gas Turbine Power 2002;124:248–55.
[23] Burger M, Schmehl R, Prommersberger K, Schäfer O, Koch R, Wittig S. Droplet evaporation modeling by the distillation curve model: accounting for kerosene fuel and elevated pressures. Int J Heat Mass Transfer 2003;46:4403–12.
[24] Rätzsch MT, Kehlen H. Continuous thermodynamics of complex mixtures. Fluid Phase Equilib 1983;14:225–34.
[25] Cotterman RL, Bender R, Prausnitz JM. Phase equilibria for mixtures containing very many components: development and application of continuous thermodynamics for chemical process design. Ind Eng Chem Proc Des Dev 1985;24:194–203.
[26] Tamim J, Hallett WLH. A continuous thermodynamics model for multicomponent droplet vaporization. Chem Eng Sci 1995;50:2933–42.
[27] Zhu-sheng G, Reitz RD. A model for high-pressure vaporization of droplets of complex liquid mixtures using continuous thermodynamics. Int J Heat Mass Transfer 2002;45:495.
[28] Harstad K, Bellan J. Modeling evaporation of Jet A, JP-7, and RP-1 drops at 1 to 15 bars. Combust Flame 2004;137:163–77.
[29] Banerjee R. Turbulent conjugate heat and mass transfer from the surface of a binary mixture of ethanol/iso-octane in a countercurrent stratified two-phase flow system. Int J Heat Mass Transfer 2008;51:5958–74.
[30] Hirt CW, Nichols B. Volume of fluid (VOF) method for the dynamics of free boundaries. J Comput Phys 1981;39:201–25.
[31] Sussman M, Smereka P, Osher S. A level set approach for computing solutions to incompressible two-phase flow. J Comput Phys 1994;114:146–59.
[32] Unverdi SO, Tryggvason G. A front-tracking method for viscous, incompressible, multi-fluid flows. J Comput Phys 1992;100:25–37.
[33] Ménard T, Tanguy S, Berlemont A. Coupling level set/VOF/ghost fluid methods: validation and application to 3D simulation of the primary break-up of a liquid jet. Int J Multiphase Flow 2007;33:510–24.
[34] Wohak MG, Beer H. Numerical simulation of direct-contact evaporation of a drop rising in hot, less volatile immiscible liquid of higher density – possibilities and limits of the SOLA-VOF/CSF algorithm. Numer Heat Transfer, Part A 1998;33:561–82.
[35] Harvie DJE, Fletcher DF. A hydrodynamic and thermodynamic simulation of droplet impacts on hot surfaces, Part I : theoretical model. Int J Heat Mass Transfer 2001;44:2633–42.
[36] Davidson MR, Rudman M. Volume-of-fluid calculations of heat or mass transfer across deforming interfaces in two-fluid flow. Numer Heat Transfer, Part B 2002;41:291–308.
[37] Welch SWJ, Rachidi T. Numerical computational of film boiling including conjugate heat transfer. Numer Heat Transfer 2002;42:35–53.
[38] Agarwal DK, Welch SWJ, Biswas G, Durst F. Planar simulation of bubble growth in film boiling in near-critical water using a variant of the vof method. J Heat Transfer 2004;126:329–38.
[39] Tanguy S, Ménard T, Berlemont A. A level set method for vaporizing two-phase flows. J Comput Phys 2007;221:837–53.
[40] Schlottke J, Weigand B. Direct numerical simulation of evaporating droplets. J Comput Phys 2008;227:5217–37.
[41] Strotos G, Gavaises M, Theodorakakos A, Bergeles G. Numerical investigation of the evaporation of two-component droplets. Fuel 2011;90:1492–507.
[42] Sirignano WA, Law CK. Transient heating and liquid–phase mass diffusion in fuel droplet vaporization. In: Zung J, editor. Evaporation – combustion of fuels. Washington DC: American Chemical Society; 1978. p. 3–26.
[43] Aggarwal SK. A review of spray ignition phenomena: present status and future research. Prog Energy Combust Sci 1998;24:565–600.
[44] Sazhin SS. Advanced models of fuel droplet heating and evaporation. Prog Energy Combust Sci 2006;32:162–214.
[45] Banerjee R, Gopinath R. CFD analysis to study evaporation of a single ethanol/iso-octane binary mixture droplet. In: AJK2011-FED, Hamamatsu, Japan; 2011.

[46] Brackbill JU, Kothe DB, Zemach C. A continuum method for modeling surface tension. J Comput Phys 1992;100:335–54.
[47] Banerjee R. A numerical study of combined heat and mass transfer in an inclined channel using the VOF multiphase model. Numer Heat Transfer, Part A 2007;52:163–83.
[48] Poling BE, Prausnitz JM, O'Connell JP. The properties of gases and liquids. 5th ed. New York: McGraw-Hill; 2000.
[49] Daïf A, Bouaziz M, Chesneau X, Chérif AA. Comparison of multicomponent fuel droplet vaporization experiments in forced convection with the Sirignano model. Exp Therm Fluid Sci 1999;18:282–90.